Biophysical Influence of Airborne Carbon Nanomaterials on Natural Pulmonary Surfactant

Russell P. Valle,[†] Tony Wu,[†] and Yi Y. Zuo*[,†,‡]

[†]Department of Mechanical Engineering, University of Hawaii at Mnoa, Honolulu, Hawaii 96822, United States and [‡]Department of Pediatrics, John A. Burns School of Medicine, University of Hawaii, Honolulu, Hawaii 96826, United States

ABSTRACT Inhalation of nanoparticles (NP), including lightweight airborne carbonaceous nanomaterials (CNM), poses a direct and systemic health threat to those who handle them. Inhaled NP penetrate deep pulmonary structures in which they first interact with the pulmonary surfactant (PS) lining at the alveolar air–water interface. In spite of many research efforts, there is a gap of knowledge between *in vitro* biophysical study and *in vivo* inhalation toxicology since all existing biophysical models handle NP–PS interactions in the liquid phase. This technical limitation, inherent in current *in vitro* methodologies, makes it impossible to simulate how airborne NP deposit at the PS film and interact with it. Existing *in vitro* NP–PS studies using liquid-suspended particles have been shown to artificially inflate the no-observed adverse effect level of NP exposure when compared to *in vivo* inhalation studies and international occupational exposure limits (OELs). Here, we developed an *in vitro* methodology called the constrained drop surfactometer (CDS) to quantitatively study PS inhibition by airborne CNM. We show that airborne multiwalled carbon nanotubes and graphene nanoplatelets induce a concentration-dependent PS inhibition under physiologically relevant conditions. The CNM aerosol concentrations controlled in the CDS are comparable to those defined in international OELs. Development of the CDS has the potential to advance our understanding of how submicron airborne nanomaterials affect the PS lining of the lung.

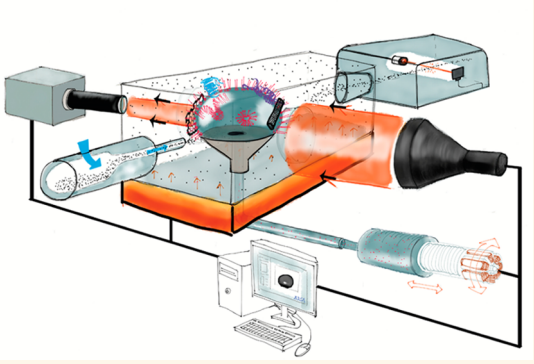

KEYWORDS: pulmonary surfactant · nanoparticle · aerosol · constrained drop surfactometer · carbon nanotube · graphene nanoplatelet

The development of engineered nanomaterials has flourished in recent decades. Carbonaceous nanomaterials (CNM), including carbon nanotubes (CNT) and graphene nanoplatelets (GNP), have unique characteristics that have helped innovate modern technology.[1] Their unique aspect ratios, conductivity, and physicochemical properties have brought carbon to the forefront of nanotechnology. Most notably, their sizes and aspect ratios give them unprecedentedly large surface area to volume ratios. This property among others of CNM has allowed researchers to push the boundaries of electronics, biomedicine, and many other applications.[1] However, the same attributes of CNM that give them a broad spectrum of applications also pose potential health hazards to those who handle them.[2,3]

Both CNT and GNP are lightweight and easily airborne. One of the serious risks when working with nanomaterials is particle inhalation. Inhaled nanoparticles (NP) have been reported to cause damage to respiratory, cardiovascular, neurological, hepatic, and gastrointestinal tissues.[4] Due to their small size, when inhaled, NP penetrate deep and deposit primarily in the alveolar region of the lung.[5] Studies have shown that inhaled NP, including CNM, disrupt lung function by increasing oxidative stress and inflammation and can ultimately cause carcinomas.[4–6]

The entirety of the peripheral lung is lined with a lipid–protein pulmonary surfactant (PS) complex.[7] PS serves two major functions in the lung. The first is innate immunity, *i.e.*, being the initial biological barrier for any air contaminants that may reach the deep lung. The second is its biophysical function that allows for normal lung mechanics and prevents alveolar collapse by

* Address correspondence to yzuo@hawaii.edu.

Received for review February 20, 2015 and accepted May 1, 2015.

Published online May 01, 2015
10.1021/acsnano.5b01181

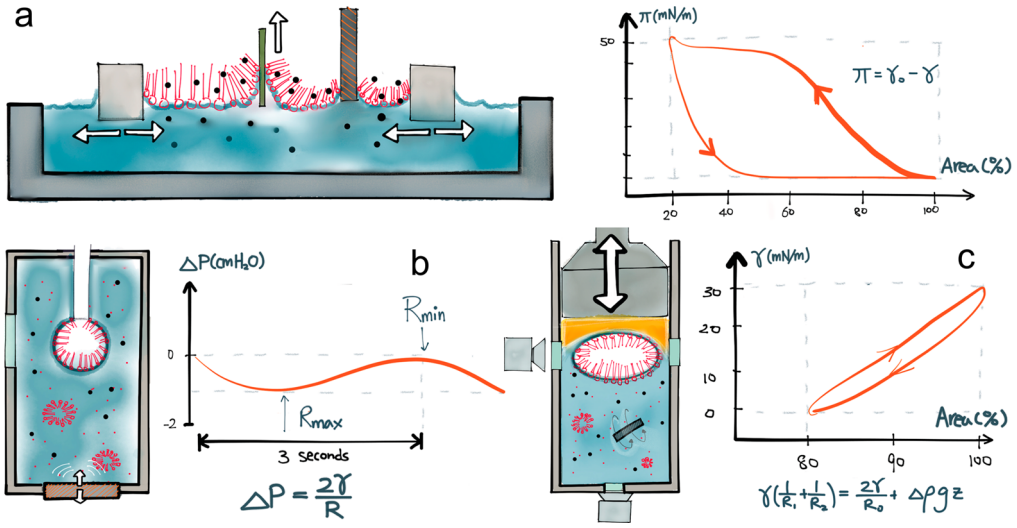

Figure 1. Schematics and typical outputs of *in vitro* experimental methodologies used in the literature for studying pulmonary surfactant (PS) interaction with nanoparticles (NP). (a) Langmuir trough in which NP are either cospread with PS at the air−water interface or dispersed/injected in the aqueous subphase. Surfactant films at the air−water interface can be Langmuir−Blodgett (LB) transferred onto a solid substrate for microscopy imaging. Due to their large size, Langmuir trough experiments are usually performed under ambient environment. Surface pressure ($\pi = \gamma_0 - \gamma$ in which γ_0 is the surface tension of air−water interface) is determined with a Wilhelmy plate in contact with the air−water interface. This limits the rate of film compression as quick compression generates waves at the surface, interfering with the surface pressure measurement. The Langmuir trough is usually only used for studying compression as the surface pressure decreases steeply upon the initial expansion, resulting in a large hysteresis area for the compression−expansion loop. Sudden drop of surface pressure, *i.e.*, rapid increase of surface tension, at low lung volumes would result in disorganization of the delicate alveolar tissue and cause alveolar collapse. Hence, the Langmuir trough is incapable of mimicking biophysical properties of natural PS. (b) Pulsating bubble surfactometer (PBS) in which NP are first mixed with the PS suspension and subsequently exposed to a ~1 mm air bubble suspending at a capillary tube open to the atmosphere. The bubble is oscillated between two fixed radii by drawing air into the bubble, usually at 20 cycles/min with a maximum 50% variation in its surface area. Surface tension (γ) is estimated from the negative pressure caused by the pulsator, *i.e.*, the pressure difference across the bubble surface (ΔP), using the Laplace equation for a spherical surface, $\Delta P = 2\gamma/R$. (c) Captive bubble surfactometer (CBS) in which NP are first mixed with the PS suspension and subsequently exposed to an air bubble of ~5 mm in diameter. The bubble floats against a hydrophilic ceiling usually made of 1% agarose gel. The hydrophilic ceiling adsorbs a thin aqueous wetting film that prevents the bubble from physically touching the solid surface, thus maintaining the integrity of the "captive" bubble and entirety of the air−water interface. The surfactant subphase is stirred to maintain an adsorption-controlled environment. The bubble is oscillated by varying hydraulic pressure of the subphase with tunable rates of cycling and amounts of compression. The surface tension is determined by analyzing the shape of the captive bubble, *e.g.*, numerically solving the classical Laplace equation of capillarity $\gamma((1/R_1) + (1/R_2)) = (2\gamma/R_0) + \Delta\rho gz$, in which R_1 and R_2 are the two principal radii of curvature at any point of the bubble surface; R_0 is the radius of curvature at the bubble apex; $\Delta\rho$ is the density difference across the bubble surface. The CBS has been proven to be a benchmark for simulating biophysical properties of natural PS, such as rapid adsorption, low film compressibility upon compression, and rapid readsorption upon expansion.

reducing the surface tension. Its ability in reducing surface tension is attributed to the high phospholipid content as well as the two hydrophobic surfactant proteins associated with PS: SP-B and SP-C.[8] By reducing the alveolar surface tension to near-zero levels, inhalation−exhalation cycles can occur at minimum mechanical energy expense.[7] When PS is inhibited, its biophysical function deteriorates leading to respiratory ailments including acute lung injury (ALI) and even acute respiratory distress syndrome (ARDS).[9]

A wealth of *in vitro* studies, including our own, have demonstrated that the biophysical function of PS can be inhibited by NP.[10−20] The degree of biophysical inhibition depends on the physicochemical characteristics of the NP, such as their size, shape, charge, hydrophobicity, and agglomeration state.[10−20] Although providing certain physiological insight into the interaction between PS and inhaled NP, all previous *in vitro* studies suffer from the technical limitation that the NP must be brought into contact with PS from a liquid phase. When studying hydrophilic NP, the NP are usually dispersed in an aqueous buffer and then mixed with the PS suspension.[13−16] When studying hydrophobic NP, the NP are commonly dispersed in an organic solvent and subsequently spread atop the PS suspension, or cospread with organic-extracted PS.[10−12]

These NP handling techniques are largely limited by the *in vitro* experimental methodologies used in previous studies, including the Langmuir trough,[10−14] pulsating bubble surfactometer (PBS),[15−17] and captive bubble surfactometer (CBS).[18,19] Figure 1 shows the schematics of the Langmuir trough, PBS,[21] and CBS[22] for studying NP−PS interactions. It can be seen that these *in vitro* methods fail to mimic the true physiological conditions of NP−PS interactions, where the adsorbed PS films at the alveolar interface interact with NP deposited from the air. Consequently, extrapolating available *in vitro* data to *in vivo* tests has

achieved only limited success. Physiologically irrelevant large NP concentrations are usually needed to induce *in vitro* surfactant inhibition.

In this study, we have developed a novel experimental methodology called the constrained drop surfactometer (CDS) to fully simulate nano-bio interactions between natural PS and airborne CNM. We will show that the CDS can be used as an ideal *in vitro* biophysical model to mimic the physiological condition of respiration. The CDS offers, for the first time, quantitative correlations between airborne CNM and aerosol-induced PS inhibition under physiologically relevant conditions. With a novel *in situ* Langmuir–Blodgett (LB) transfer technique, the CDS permits direct visualization of nano-bio interaction at the PS interface, thus allowing for mechanism studies of surfactant inhibition by airborne CNM. The development of the CDS has made it possible to better understand how submicron airborne nanomaterials affect the PS lining of the lung.

RESULTS AND DISCUSSION

CDS Development. Figure 2 shows a schematic of the CDS setup. The CDS simulates the air–water interface of the alveolar lining using a surfactant droplet (~10 μL) on which a surfactant film is quickly formed by natural adsorption, indicated by reaching the equilibrium surface tension of ~25 mN/m within a few seconds.[7] The droplet is constrained onto a 3 mm hydrophilic pedestal with a knife-sharp edge, which prevents leakage of the surfactant film even at substantially low, near-zero surface tensions upon compression.[23] Formation, oscillation, and removal of the droplet are controlled by a programmable motorized syringe. This droplet is illuminated by a backlight, while a high-definition camera continuously records images of the droplet profile. Drop images are processed using an upgraded axisymmetric drop shape analysis (ADSA) algorithm that automatically determines the surface tension, surface area, and drop volume from the shape of the droplet.[20,24] To mimic pulmonary conditions, the surfactant droplet is enclosed in an environmental control chamber, which maintains the core body temperature (37.0 ± 0.1 °C). The maximum spatial temperature variation in the chamber is less than 0.5 °C, as shown in Figure S7 of the Supporting Information. The relative humidity (RH) in the chamber is maintained at ~85%, which is sufficiently high in simulating the pulmonary condition[25,26] while not interfering with aerosol counting using laser diffraction. To simulate respiration, the adsorbed surfactant film is periodically compressed and expanded by precisely controlling liquid flow into and out of the droplet at a rate of 20 cycles per minute with area variations no more than 20%, all mimicking normal tidal breathing.[27]

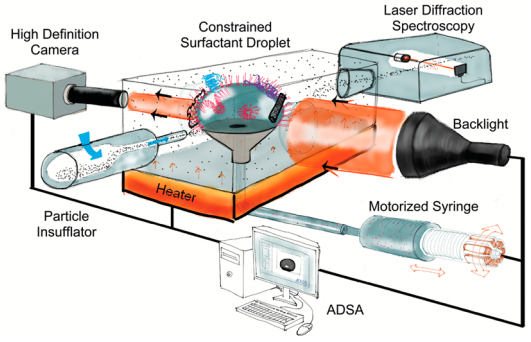

Figure 2. Schematic of the constrained drop surfactometer (CDS) for studying biophysical influence of airborne carbon nanomaterials (CNM) on pulmonary surfactant (PS). A PS droplet is formed on a 3 mm hydrophilic knife-sharp pedestal using a programmable motorized syringe. This droplet is enclosed in an environmental control chamber where core body temperature is maintained with a thermoelectric heater. The drop profile is illuminated with a monochromic parallel backlight and is recorded continuously with a high-definition camera. The profile images are sent directly to the axisymmetric drop shape analysis (ADSA) software and processed to yield real-time surface tension measurements. CNM is aerosolized into the chamber using a particle insufflator. The airborne particle size distribution is determined with laser diffraction spectroscopy using a particle counter. The environmental control chamber and all tubing are airtight to ensure no particle leakage.

The importance of simulating <20% area variations should be emphasized as numerous lung physiological studies have convincingly demonstrated that variation in alveolar surface area is small during normal breathing.[27–29] Surface area of the lung does not change more than 30% during a deep breath between 40 and 100% total lung capacity (TLC). During normal tidal breathing between 40 and 50% TLC, the area variation is less than 10% which is associated with a minimal surface tension change barely more than 5 mN/m.[27–29] All this physiological evidence suggests that the natural PS films must have a very low compressibility contributing to lung recoil. It is therefore important to control these physiological conditions during *in vitro* biophysical simulations.

Figure 3 shows a surface tension (γ) *versus* relative surface area (A) plot of a typical compression–expansion cycle of an adsorbed Infasurf film, recorded in ambient air as a control. The inserts show representative droplet images at various surface tensions. It can be seen that the surface tension reaches a value lower than 5 mN/m with less than 20% film compression, indicating a "strong" surfactant film with a low compressibility. When the surfactant film is expanded, the surface tension gradually increases to follow the path of compression, thus minimizing the hysteresis loop. This gradual increase in surface tension indicates a "soft" film that is efficiently replenished by surfactant readsorption during expansion. Hence, the CDS successfully simulates the soft-yet-strong biophysical property of natural PS film under physiologically relevant conditions. (Video 1 in the Supporting Information shows a demo for repeated compression–expansion

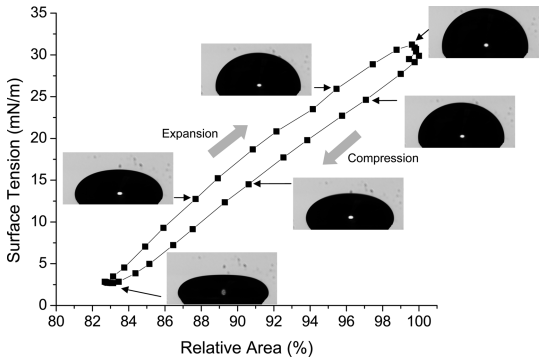

Figure 3. Typical compression−expansion cylce for pure Infasurf at 37 °C and 20 cycles/min determined using the contrained drop surfactomter (CDS). Infasurf reaches a minimum surface tension below 5 mN/m within 20% relative area compression, indicating high surface activity. The compression−expansion hysteresis loop is narrow stemming from the compressibility of the film being almost equivalent to its expandability. It means that during each compression−expansion cycle there is a minimal mechanical energy expense, which is crucial for maintaining the normal respiratory mechanics. Surface tension was determined using axisymmetric drop shape analysis (ADSA). The drop images along the cycle path are demonstrative of how surface tension is a function of the drop shape.

cycles of an Infasurf droplet. It can be seen that when the surfactant film is compressed the droplet flattens due to a decrease in surface tension.) To further demonstrate the accuracy of the CDS in simulating biophysical properties of natural PS, Figure S8 compares the compression−expansion isotherms of Infasurf produced using the Langmuir trough, CBS, and CDS, respectively. Figure S9 compares the minimum surface tension (γ_{min}) of a clinical surfactant preparation, Curosurf (at 1.5 mg/mL), evaluated under physiologically relevant conditions using the PBS[15] and the CDS, respectively. Both comparisons demonstrate excellent agreement between the CDS and established methods, such as the PBS and CBS.

To introduce CNM aerosols, a miniscule amount of CNT or GNP (~0.1 mg) is loaded into a dry powder insufflator (Penn-Century, Inc., Glenside, PA) and subsequently insufflated into the environmental control chamber. The airborne particle size distribution in the chamber is determined with laser diffraction spectroscopy (LDS). After insufflation, the airborne CNM are allowed 30 min to settle naturally before forming the surfactant droplet. As shown in Figure S1, this settling process eliminates most airborne particles larger than 2.5 μm, thus forming a relatively uniform aerosol distribution in the chamber. Figure 4 shows the stabilized aerosol distributions of CNT and GNP. 99% of airborne CNT and 98% of airborne GNP particles have an aerodynamic size of less than 2.5 μm. A large majority (84% and 63%) of these airborne particles lie in the submicron (300−500 nm) range. To facilitate comparison with existing *in vivo* and occupational safety data, the particle number concentration

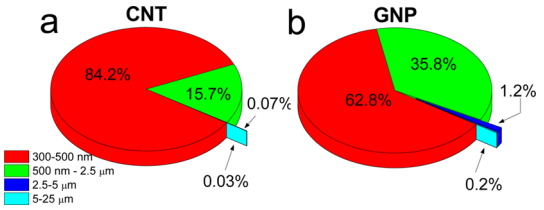

Figure 4. CNT (a) and GNP (b) aerosol size distributions 30 min after initial aerosolization. A large majority of both CNT (99%) and GNP (>98%) aerosol aggregates are less than 2.5 μm. Most of the aerosols less than 2.5 μm for CNT (84%) and GNP (63%) are in the submicron range (300−500 nm). Larger, coarse aggregates make up less than 1% and 2% of the aerosols in the chamber for CNT and GNP, respectively.

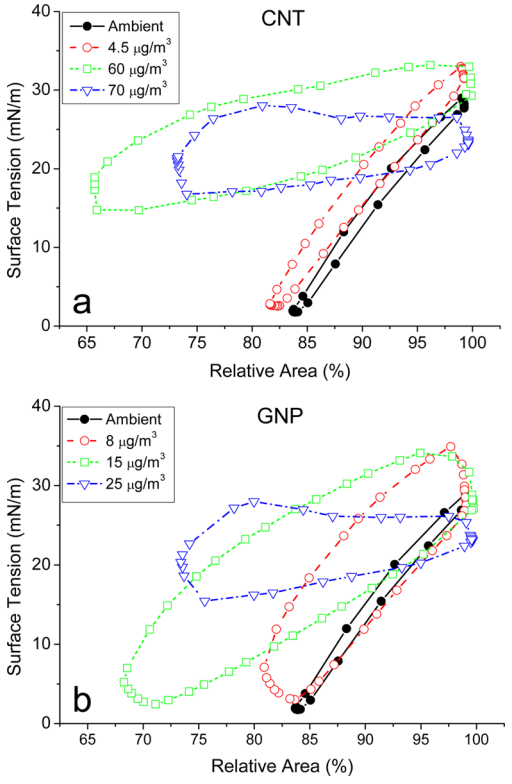

Figure 5. Comparison of dynamic cycling of Infasurf exposed to CNT (a) or GNP (b) with increasing aerosol concentration. Each plot demonstrates a representative compression−expansion cycle of Infasurf exposed to ambient air and increasing concentration of CNM aerosols. For both cases, increasing CNM aerosol concentration increased the minimum surface tension upon compression and increased the hysteresis area of the compression−expansion loops, indicating surfactant inhibition.

determined by LDS is converted to particle mass concentration (μg/m^3) using a standard approach.[30]

CNM Aerosol-Induced Surfactant Inhibition. Once the airborne particle distribution is stabilized (Figure 4), an Infasurf droplet is formed atop the CDS pedestal, incubated in the aerosols for 10 min, and then subjected to compression−expansion cycles to simulate respiration in the polluted environment. Figure 5 shows representative cycles for Infasurf exposed to ambient air and three increasing concentrations of the

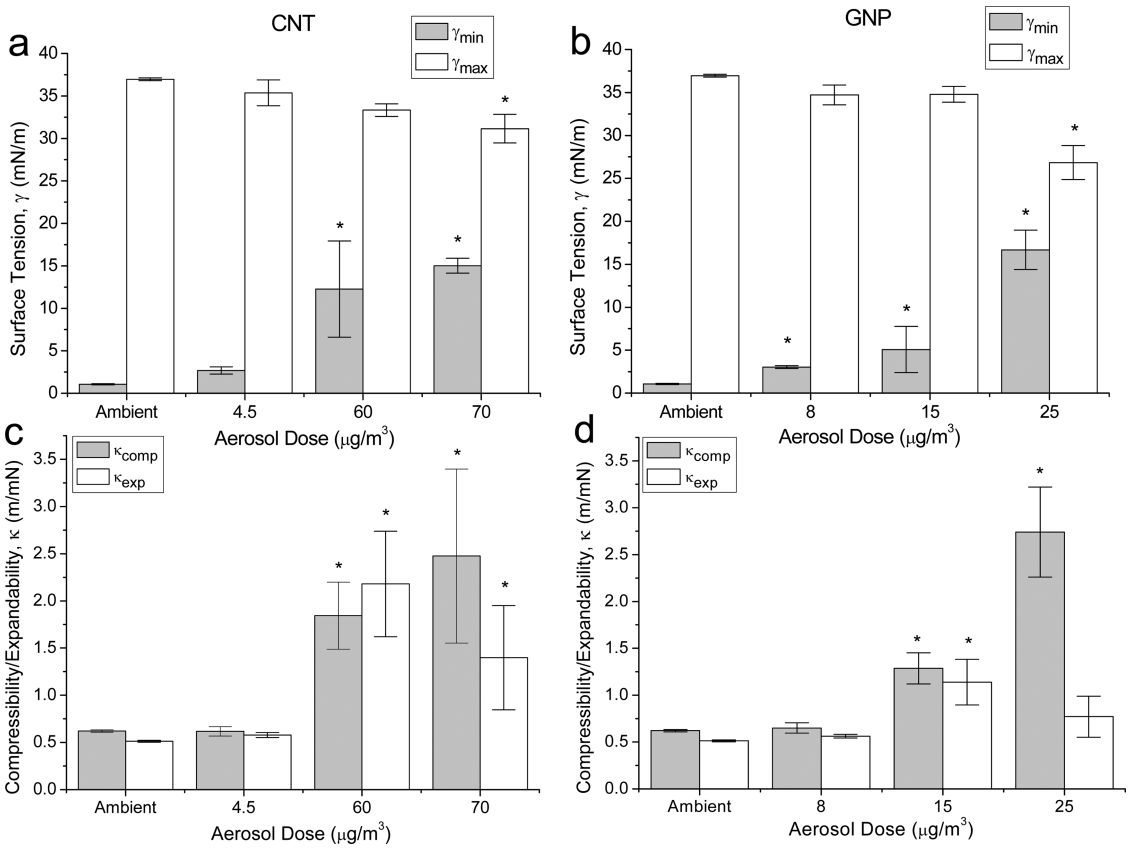

Figure 6. Statistical analysis of biophysical properties of Infasurf exposed to CNT (a, c) or GNP (b, d) with increasing aerosol concentration. These four biophysical properties are the minimum surface tension at the end of compression (γ_{min}), maximum surface tension at the end of expansion (γ_{max}), film compressibility (κ_{comp}), and film expandability (κ_{exp}). All cycles were produced at 37 °C and 3 s/cycle to mimic respiration. There is a statistically significant increase in both γ_{min} and κ_{comp} after exposure to aerosol concentrations greater than 20 μg/m^3, indicating surfactant inhibition. *$p < 0.05$ of comparison to ambient air control.

CNM, *i.e.*, 4.5 ± 0.4, 60 ± 18, and 70 ± 18 μg/m^3 for CNT and 8.0 ± 1.7, 15 ± 3, and 25 ± 6 μg/m^3 for GNP. (Reproducibility of these cycles can be found in Figures S2 and S3 of the Supporting Information.) It is clear that the biophysical properties of Infasurf are inhibited by the airborne CNM in a concentration dependent manner, as indicated by the inability of reaching low surface tension upon 20% relative area compression and the increasing hysteresis area of the compression−expansion loops. (Note that when exposing to CNM aerosols, we increased the amount of film compression to 30% to examine the extent of surfactant inhibition.) Movies of compression−expansion cycles for the Infasurf droplets exposed to CNT and GNP are given in videos 2 and 3, respectively. Surfactant inhibition is indicated by the high-curvature drop shape at the end of compression, indicating high surface tensions.

To gain a statistical understanding of surfactant inhibition caused by the CNM aerosols, Figure 6 shows four statistical parameters to quantify surfactant biophysics and inhibition. These are the minimum surface tension after compression (γ_{min}), maximum surface tension after expansion (γ_{max}), film compressibility (κ_{comp}), and film expandability (κ_{exp}) with and without exposure to CNM aerosols. A good surfactant should reduce surface tension below 5 mN/m with under 20% relative area compression,[27,31] as shown by the ambient air control (Figure 3). Upon CNM exposure, γ_{min} rises considerably in a dose-dependent manner from ~2 mN/m when exposed to the ambient air, to >10 mN/m after exposure to higher than 20 μg/m^3 for both CNT and GNP.

In contrast to γ_{min}, the compressibility (κ_{comp}) and expandability (κ_{exp}) of surfactant films, defined as $\kappa = (1/A)(\partial A/\partial\gamma)$ during the compression and expansion processes, are more sensitive parameters for measuring surfactant inhibition.[20,31] Increasing κ_{comp} correlates with a softer film, which requires more compression to ultimately reach the same γ_{min}, *i.e.*, surfactant inhibition. As shown by both CNM, κ_{comp} increases with increasing aerosol concentration. Additionally, the hysteresis loop associated with surfactant inhibition is caused by the difference between κ_{comp} and κ_{exp}. When these two values are identical it yields zero hysteresis, *i.e.*, expansion path retraces compression path as shown by the ambient air control, indicating no mechanical energy expense per respiration

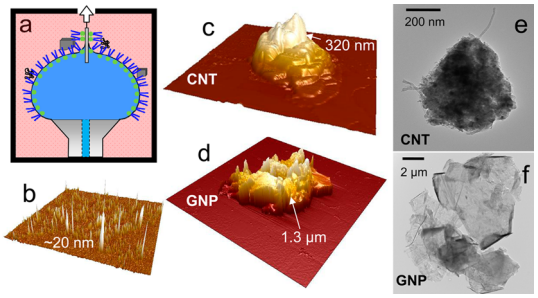

Figure 7. Imaging nano-bio interactions at the PS film. (a) Schematic of the *in situ* Langmuir–Blodgett (LB) transfer technique integrated into the CDS. The surfactant film at the air–water interface of the droplet is transferred onto a small piece of freshly peeled mica sheet at a lifting speed of 1 mm/min, under controlled environmental conditions in the chamber. (b) AFM topographic image (20 × 20 μm) of a pure Infasurf film that shows uniformly distributed multilayer structures. (c, d) AFM topographic images of the Infasurf film exposed to CNT (10 × 10 μm) and GNP (20 × 20 μm) aerosols, respectively. Both images show the adsorption of large aggregates onto the surfactant film. (e, f) TEM images of CNT and GNP aerosols recovered from the chamber. Both size and morphology of these CNM aerosols match the large aggregates found at the surfactant film.

cycle.[20,31] However, after exposure to the highest concentration of CNM, κ_{comp} and κ_{exp} show large differences (Figure 6) and thus increasing hysteresis area (Figure 5), indicating loss of mechanical energy which is ultimately unsustainable and will lead to respiratory failure.

***In Situ* LB Transfer and Film Imaging.** To explore the mechanism of surfactant inhibition, we have developed a novel *in situ* Langmuir–Blodgett (LB) transfer technique that allows us to immobilize the adsorbed surfactant film at the droplet surface under controlled environment, thus probing the nano-bio interactions with submicron resolution using atomic force microscopy (AFM). Before transferring the surfactant film, we first wash away surfactant vesicles in the droplet with buffer using a subphase replacement technique.[32] This is implemented by using a coaxial CDS pedestal connected to two motorized syringes, with one withdrawing the surfactant-containing subphase and meanwhile another one injecting buffer into the droplet. Integrity of the *de novo* adsorbed surfactant film after subphase replacement is examined by comparing the compression–expansion isotherms before and after the subphase replacement (Figure S10, Supporting Information). After the subphase replacement, the surfactant film at the air–water interface of the droplet is transferred onto a small piece of freshly peeled mica sheet, under controlled environmental conditions in the chamber (see Figure 7a for schematic).

As shown in Figure 7b, pure Infasurf after *de novo* adsorption shows uniform multilayer protrusions of ~20 nm, which is in good agreement with the microstructure of spread Infasurf film around the equilibrium spreading pressure.[33,34] However, after exposure to CNT or GNP, large aggregates appear on the surfactant film (Figure 7c,d) within the aerosol size range reported by LDS (Figure 4). To further scrutinize these aggregates, we have directly studied the morphology of CNM aerosols collected from the environmental control chamber, using TEM. As shown in Figure 7e, CNT form fibrous or isometric aerosols where tubes entangle with each other, very similar to the CNT "birdnest" structures after aerosolization, reported by others.[35] GNP form large platelet aggregates with multiple sheets stacked onto each other as shown in Figure 7f. (See Figures S4–S6 in the Supporting Information for additional AFM and TEM images.)

It is clear that both size and morphology of these CNM aerosols are comparable to the aggregates found at the surfactant film (Figure 7c–f), which confirms that nano- and micron-sized airborne CNM deposit at the surfactant film where nano-bio interactions take place inducing surfactant inhibition. These results are in good agreement with previous *in vitro* and *in silico* studies that show hydrophobic NP adsorb to the surfactant film where the nano-bio interactions govern the surfactant inhibition.[11,12,14,20]

CNT Occupational Exposure Limit Analysis. The CDS proved to be a sensitive tool for studying aerosol-induced surfactant inhibition. More importantly, it demonstrates the potential as an *in vitro* model for studying inhalation toxicology with controlled aerosol dosimetry. Worldwide airborne CNT occupational exposure limits (OELs) range from 7 to 50 μg/m^3.[36] In Japan, several studies using mice models showed no-observed adverse effect level at 65 μg/m^3.[37,38] However, after adjusting to human exposure they determined the OEL for multiwalled CNT to be 30 μg/m^3. In contrast, the National Institute of Occupational Safety and Health (NIOSH) has recommended CNT OEL standards to a more conservative 7 μg/m^3 in the United States based on chronic inhalation studies.[39,40] Although there are differences between international OELs, they are around 10–50 μg/m^3. Previous NP–PS *in vitro* studies recorded PS inhibition at NP concentrations from 10 μg/mL to 2 mg/mL.[10–20] These doses are astronomically larger than the international standards. In contrast, these international OELs fall directly in the detection range of the CDS.

In agreement with NIOSH, we found negligible adverse biophysical influences for CNT and GNP below 8 μg/m^3. Slightly higher concentrations show minor inhibition patterns, *i.e.*, increases in κ_{comp} (Figures 5 and 6), associated with doses below 20 μg/m^3 for both CNT and GNP. Concentrations higher than 20 μg/m^3 yielded a more severe surfactant inhibition signified by an increase γ_{min} above 5 mN/m as well as a continued increase in κ_{comp}. Hence, not only is the CDS able to control airborne concentrations in the range of international OELs, but it can also monitor the dose-dependent biophysical inhibition associated with CNM aerosol exposure.

In addition to agreeing with international standards, our *in vitro* findings also provide insight into occupational safety. Erdely et al. recently toured several U.S. manufacturing facilities and tested the airborne CNT exposure to workers.[41] The goal of their study was to provide information on human occupational exposure limits and ultimately correlate existing *in vivo* data to day-to-day workplace exposures. Of these manufacturing facilities the airborne carbon concentration they found ranged from nondetectable to >80 $\mu g/m^3$, with the average respirable CNT concentration to be 2.65 $\mu g/m^3$. The range of inhalable carbon concentration found at these sites falls directly in the testing range for the CDS in this study, showing the practical use of the CDS in studying occupational health. With these data, they were able to link worker exposure to results obtained from *in vivo* mouse inhalation models.[42−46] With our *in vitro* results we can conclude that acute exposure to this concentration of CNT will have minimal inhibitory effect on the PS system. Hence, the CDS provides a promising model for correlating *in vitro* aerosol data with *in vivo* intratracheal exposure and human occupational safety data.

Compared to CNT, much less work has been focused on the inhalation toxicology of GNP. However, the unique platelet shape of GNP has researchers asking how its inhalation toxicological potential differs from that of the fibrous CNT.[47] In a comparative CNM inhalation study, Ma-Hock et al. demonstrated that CNT and GNP showed pulmonary toxicity at different potentials; but the origin of this difference is still unknown.[46] We also found that although CNT and GNP both inhibit PS at increasing concentration and both adsorb to the PS film, their inhibition potentials were not identical. There are many parameters that may affect this difference in the inhibitory potential such as the chemical reactivity at the nanoaggregate surface, adsorption kinetics, and agglomeration morphology. The reason for this difference is currently under investigation.

CONCLUSIONS

We have developed an *in vitro* experimental model called the constrained drop surfactometer (CDS) capable of quantitatively evaluating surfactant inhibition caused by airborne nanomaterials. Both CNM tested, CNT and GNP, demonstrated a concentration dependent surfactant inhibition under physiologically relevant conditions. With a unique *in situ* LB transfer technique, the CDS demonstrated that surfactant inhibition was caused by the adsorption of CNM aerosols onto the surfactant film, which disturbed molecular conformation and film structure of the PS. The CDS exhibits promises to be developed into a precautionary tool for evaluating surfactant inhibition and ultimately for studying inhalation toxicology due to airborne nanomaterials.

METHODS

Pulmonary Surfactant. We used an animal-derived PS, Infasurf (Calfactant), which was a gift from ONY Inc. (Amherst, MA). Infasurf was purified from whole-lung bronchopulmonary lavage of newborn calves. Through an extraction process, Infasurf retained all of the hydrophobic components of bovine endogenous surfactant including phospholipids, cholesterol, and most hydrophobic surfactant proteins (SP-B and SP-C).[34] For all trials, Infasurf was diluted to a phospholipid concentration of 0.5 mg/mL with a saline buffer of 0.9% NaCl, 1.5 mM $CaCl_2$, and 2.5 mM HEPES, adjusted to pH 7.0. The saline buffer was made with Milli-Q ultrapure water (Millipore, Billerica, MA) with a resistivity greater than 18 MΩ·cm at room temperature.

Carbon Nanomaterials. Multiwalled CNT with a length of 1−5 μm and diameter of 30 ± 15 nm was purchased from NanoLab Inc. (Waltham, MA). GNP with a sheet length of 5 μm and a thickness of 6−8 nm was purchased from Strem Chemicals Inc. (Newburyport, MA). All CNM were thoroughly characterized for purity and morphology before use.

Aerosol Concentration Determination. The airborne particle number concentration in the chamber was determined with laser diffraction spectroscopy (LDS) using an AeroTrak airborne particle counter (TSI Inc., Shoreview, MN). The particle number concentration was subsequently converted to the particle mass concentration using a standard approach[30] by assuming a spherical shape and an aerosol density of 0.07 g/cm^3, which is much less than the density of bulk CNM.[35] Low, moderate, and high exposure levels were produced in experiments by loading and in turn aerosolizing the CNM multiple times. Concentration for each exposure level was measured in triplicate. Detailed conversion and reproducibility are summarized in Table S1, Supporting Information.

AFM. Topographical images were obtained using an Innova AFM (Bruker, Santa Barbara, CA). Samples were scanned in air where both tapping mode and contact mode gave identical results. A silicon nitride cantilever with a spring constant of 0.12 N/m and a tip radius of 2 nm was used in contact mode. In tapping mode a resonance frequency of 300 kHz and spring constant of 40 N/m was used. Lateral structures were analyzed and 3-dimensional rendering were produced using Nanoscope Analysis (version 1.5). Images were taken at multiple positions to ensure reproducibility.

TEM. Both CNT and GNP were characterized with TEM (Hitachi HT7700). To find aerosol aggregate size and morphology, TEM grids were placed at the purging port of the CDS chamber *prior to* insufflations. Once in place, the CNM was aerosolized in the chamber and allotted 30 min to allow larger aggregates to settle. The chamber was purged, and these grids were subsequently visualized *via* TEM within 24 h of aggregate collection.

Statistical Analysis. Statistical data are represented by the mean ± standard deviation. The measurements are based on dynamic cycling data for ambient air control and three increasing concentrations all with a sample size of $n = 3$. One-way ANOVA was used for statistical calculations (OriginPro, Northampton, MA). The Tukey means comparison test was used, and a probability value of $p < 0.05$ was considered statistically significant.

Conflict of Interest: The authors declare no competing financial interest.

Supporting Information Available: Figures S1−S10 and Table S1. Videos of Infasurf cycling exposed to ambient air, CNT, and GNP. The Supporting Information is available free of charge on the ACS Publications website at DOI: 10.1021/acsnano.5b01181.

Acknowledgment. We thank Dr. Walter Klein at ONY Inc. for donation of Infasurf samples. This work was supported by NSF Grant No. CBET-1236596 (Y.Y.Z.) and the Robert C. Perry Fund of the Hawai'i Community Foundation (Grant No. 12ADVC-51367, Y.Y.Z.). Y.Y.Z. also acknowledges support from the LNM open fund.

REFERENCES AND NOTES

1. De Volder, M. F.; Tawfick, S. H.; Baughman, R. H.; Hart, A. J. Carbon Nanotubes: Present and Future Commercial Applications. *Science* **2013**, *339*, 535–539.
2. Sanchez, V. C.; Jachak, A.; Hurt, R. H.; Kane, A. B. Biological Interactions of Graphene-Family Nanomaterials: An Interdisciplinary Review. *Chem. Res. Toxicol.* **2011**, *25*, 15–34.
3. Liu, Y.; Zhao, Y.; Sun, B.; Chen, C. Understanding the Toxicity of Carbon Nanotubes. *Acc. Chem. Res.* **2012**, *46*, 702–713.
4. Xia, T.; Li, N.; Nel, A. E. Potential Health Impact of Nanoparticles. *Annu. Rev. Public Health* **2009**, *30*, 137–150.
5. Oberdorster, G.; Oberdorster, E.; Oberdorster, J. Nanotoxicology: An Emerging Discipline Evolving from Studies of Ultrafine Particles. *Environ. Health Perspect.* **2005**, *113*, 823–839.
6. Nel, A. E.; Madler, L.; Velegol, D.; Xia, T.; Hoek, E. M.; Somasundaran, P.; Klaessig, F.; Castranova, V.; Thompson, M. Understanding Biophysicochemical Interactions at the Nano-Bio Interface. *Nat. Mater.* **2009**, *8*, 543–557.
7. Zuo, Y. Y.; Veldhuizen, R. A.; Neumann, A. W.; Petersen, N. O.; Possmayer, F. Current Perspectives in Pulmonary Surfactant-Inhibition, Enhancement and Evaluation. *Biochim. Biophys. Acta* **2008**, *1778*, 1947–1977.
8. Lopez-Rodriguez, E.; Perez-Gil, J. Structure-Function Relationships in Pulmonary Surfactant Membranes: From Biophysics to Therapy. *Biochim. Biophys. Acta* **2014**, *1838*, 1568–1585.
9. Lewis, J. F.; Veldhuizen, R. The Role of Exogenous Surfactant in the Treatment of Acute Lung Injury. *Annu. Rev. Physiol.* **2003**, *65*, 613–642.
10. Harishchandra, R. K.; Saleem, M.; Galla, H. J. Nanoparticle Interaction with Model Lung Surfactant Monolayers. *J. R. Soc. Interface* **2010**, *7*, S15–S26.
11. Sachan, A. K.; Harishchandra, R. K.; Bantz, C.; Maskos, M.; Reichelt, R.; Galla, H. J. High-Resolution Investigation of Nanoparticle Interaction with a Model Pulmonary Surfactant Monolayer. *ACS Nano* **2012**, *6*, 1677–1687.
12. Tatur, S.; Badia, A. Influence of Hydrophobic Alkylated Gold Nanoparticles on the Phase Behavior of Monolayers of DPPC and Clinical Lung Surfactant. *Langmuir* **2012**, *28*, 628–639.
13. Fan, Q.; Wang, Y. E.; Zhao, X.; Loo, J. S.; Zuo, Y. Y. Adverse Biophysical Effects of Hydroxyapatite Nanoparticles on Natural Pulmonary Surfactant. *ACS Nano* **2011**, *5*, 6410–6416.
14. Hu, G.; Jiao, B.; Shi, X.; Valle, R. P.; Fan, Q.; Zuo, Y. Y. Physicochemical Properties of Nanoparticles Regulate Translocation across Pulmonary Surfactant Monolayer and Formation of Lipoprotein Corona. *ACS Nano* **2013**, *7*, 10525–10533.
15. Schleh, C.; Muhlfeld, C.; Pulskamp, K.; Schmiedl, A.; Nassimi, M.; Lauenstein, H. D.; Braun, A.; Krug, N.; Erpenbeck, V. J.; Hohlfeld, J. M. The Effect of Titanium Dioxide Nanoparticles on Pulmonary Surfactant Function and Ultrastructure. *Respir. Res.* **2009**, *10*, 90.
16. Beck-Broichsitter, M.; Ruppert, C.; Schmehl, T.; Guenther, A.; Betz, T.; Bakowsky, U.; Seeger, W.; Kissel, T.; Gessler, T. Biophysical Investigation of Pulmonary Surfactant Surface Properties upon Contact with Polymeric Nanoparticles *in Vitro*. *Nanomedicine* **2011**, *7*, 341–350.
17. Beck-Broichsitter, M.; Ruppert, C.; Schmehl, T.; Gunther, A.; Seeger, W. Biophysical Inhibition of Synthetic *vs.* Naturally-Derived Pulmonary Surfactant Preparations by Polymeric Nanoparticles. *Biochim. Biophys. Acta* **2014**, *1838*, 474–481.
18. Bakshi, M. S.; Zhao, L.; Smith, R.; Possmayer, F.; Petersen, N. O. Metal Nanoparticle Pollutants Interfere with Pulmonary Surfactant Function *in Vitro*. *Biophys. J.* **2008**, *94*, 855–868.
19. Schurch, D.; Vanhecke, D.; Clift, M. J.; Raemy, D.; de Aberasturi, D. J.; Parak, W. J.; Gehr, P.; Petri-Fink, A.; Rothen-Rutishauser, B. Modeling Nanoparticle-Alveolar Epithelial Cell Interactions under Breathing Conditions using Captive Bubble Surfactometry. *Langmuir* **2014**, *30*, 4924–4932.
20. Valle, R. P.; Huang, C. L.; Loo, J. S. C.; Zuo, Y. Y. Increasing Hydrophobicity of Nanoparticles Intensifies Lung Surfactant Film Inhibition and Particle Retention. *ACS Sustainable Chem. Eng.* **2014**, *2*, 1574–1580.
21. Enhorning, G. Pulmonary Surfactant Function Studied with the Pulsating Bubble Surfactometer (PBS) and the Capillary Surfactometer (CS). *Comp. Biochem. Physiol. A Mol. Integr. Physiol.* **2001**, *129*, 221–226.
22. Schurch, S.; Bachofen, H.; Possmayer, F. Surface Activity *in Situ*, *in Vivo*, and in the Captive Bubble Surfactometer. *Comp. Biochem. Physiol. A Mol. Integr. Physiol.* **2001**, *129*, 195–207.
23. Yu, L. M. Y.; Lu, J. J.; Chan, Y. W.; Ng, A.; Zhang, L.; Hoorfar, M.; Policova, Z.; Grundke, K.; Neumann, A. W. Constrained Sessile Drop as a New Configuration to Measure Low Surface Tension in Lung Surfactant Systems. *J. Appl. Physiol.* **2004**, *97*, 704–715.
24. Zuo, Y. Y.; Do, C.; Neumann, A. W. Automatic Measurement of Surface Tension from Noisy Images using a Component Labeling Method. *Colloids Surf. A Physicochem. Eng. Asp.* **2007**, *299*, 109–116.
25. Zuo, Y. Y.; Gitiafroz, R.; Acosta, E.; Policova, Z.; Cox, P. N.; Hair, M. L.; Neumann, A. W. Effect of Humidity on the Adsorption Kinetics of Lung Surfactant at Air-Water Interfaces. *Langmuir* **2005**, *21*, 10593–10601.
26. Zuo, Y. Y.; Acosta, E.; Policova, Z.; Cox, P. N.; Hair, M. L.; Neumann, A. W. Effect of Humidity on the Stability of Lung Surfactant Films Adsorbed at Air-Water Interfaces. *Biochim. Biophys. Acta* **2006**, *1758*, 1609–1620.
27. Bachofen, H.; Schurch, S.; Urbinelli, M.; Weibel, E. R. Relations among Alveolar Surface Tension, Surface Area, Volume, and Recoil Pressure. *J. Appl. Physiol.* **1987**, *62*, 1878–1887.
28. Bachofen, H.; Schurch, S. Alveolar Surface Forces and Lung Architecture. *Comp. Biochem. Physiol. A Mol. Integr. Physiol.* **2001**, *129*, 183–193.
29. Kharge, A. B.; Wu, Y.; Perlman, C. E. Surface Tension *in Situ* in Flooded Alveolus Unaltered by Albumin. *J. Appl. Physiol.* **2014**, *117*, 440–451.
30. Tittarelli, A.; Borgini, A.; Bertoldi, M.; De Saeger, E.; Ruprecht, A.; Stefanoni, R.; Tagliabue, G.; Contiero, R.; Crosignani, P. Estimation of Particle Mass Concentration in Ambient Air using a Particle Counter. *Atmos. Environ.* **2008**, *42*, 8543–8548.
31. Schurch, S.; Bachofen, H.; Goerke, J.; Green, F. Surface Properties of Rat Pulmonary Surfactant Studied with the Captive Bubble Method: Adsorption, Hysteresis, Stability. *Biochim. Biophys. Acta* **1992**, *1103*, 127–136.
32. Saad, S. M.; Policova, Z.; Dang, A.; Acosta, E. J.; Hair, M. L.; Neumann, A. W. A Double Injection ADSA-CSD Methodology for Lung Surfactant Inhibition and Reversal Studies. *Colloids Surf. B Biointerfaces* **2009**, *73*, 365–375.
33. Zhang, H.; Wang, Y. E.; Fan, Q.; Zuo, Y. Y. On the Low Surface Tension of Lung Surfactant. *Langmuir* **2011**, *27*, 8351–8358.
34. Zhang, H.; Fan, Q.; Wang, Y. E.; Neal, C. R.; Zuo, Y. Y. Comparative Study of Clinical Pulmonary Surfactants Using Atomic Force Microscopy. *Biochim. Biophys. Acta* **2011**, *1808*, 1832–1842.
35. Chen, B. T.; Schwegler-Berry, D.; McKinney, W.; Stone, S.; Cumpston, J. L.; Friend, S.; Porter, D. W.; Castranova, V.; Frazer, D. G. Multi-Walled Carbon Nanotubes: Sampling Criteria and Aerosol Characterization. *Inhal. Toxicol.* **2012**, *24*, 798–820.
36. Morimoto, Y.; Horie, M.; Kobayashi, N.; Shinohara, N.; Shimada, M. Inhalation Toxicity Assessment of Carbon-Based Nanoparticles. *Acc. Chem. Res.* **2013**, *46*, 770–781.

37. Morimoto, Y.; Hirohashi, M.; Ogami, A.; Oyabu, T.; Myojo, T.; Todoroki, M.; Yamamoto, M.; Hashiba, M.; Mizuguchi, Y.; Lee, B. W.; et al. Pulmonary Toxicity of Well-Dispersed Multi-Wall Carbon Nanotubes Following Inhalation and Intratracheal Instillation. *Nanotoxicology* **2012**, *6*, 587–599.
38. Kobayashi, N.; Naya, M.; Mizuno, K.; Yamamoto, K.; Ema, M.; Nakanishi, J. Pulmonary and Systemic Responses of Highly Pure and Well-Dispersed Single-Wall Carbon Nanotubes after Intratracheal Instillation in Rats. *Inhal. Toxicol.* **2011**, *23*, 814–828.
39. Ma-Hock, L.; Treumann, S.; Strauss, V.; Brill, S.; Luizi, F.; Mertler, M.; Wiench, K.; Gamer, A. O.; van Ravenzwaay, B.; Landsiedel, R. Inhalation Toxicity of Multiwall Carbon Nanotubes in Rats Exposed for 3 Months. *Toxicol. Sci.* **2009**, *112*, 468–481.
40. Pauluhn, J. Subchronic 13-Week Inhalation Exposure of Rats to Multiwalled Carbon Nanotubes: Toxic Effects Are Determined by Density of Agglomerate Structures, Not Fibrillar Structures. *Toxicol. Sci.* **2010**, *113*, 226–242.
41. Erdely, A.; Dahm, M.; Chen, B. T.; Zeidler-Erdely, P. C.; Fernback, J. E.; Birch, M. E.; Evans, D. E.; Kashon, M. L.; Deddens, J. A.; Hulderman, T.; et al. Carbon Nanotube Dosimetry: from Workplace Exposure Assessment to Inhalation Toxicology. *Part. Fibre. Toxicol.* **2013**, *10*, 53.
42. Li, J. G.; Li, W. X.; Xu, J. Y.; Cai, X. Q.; Liu, R. L.; Li, Y. J.; Zhao, Q. F.; Li, Q. N. Comparative Study of Pathological Lesions Induced by Multiwalled Carbon Nanotubes in Lungs of Mice by Intratracheal Instillation and Inhalation. *Environ. Toxicol.* **2007**, *22*, 415–421.
43. Mitchell, L. A.; Lauer, F. T.; Burchiel, S. W.; McDonald, J. D. Mechanisms for How Inhaled Multiwalled Carbon Nanotubes Suppress Systemic Immune Function in Mice. *Nat. Nanotechnol.* **2009**, *4*, 451–456.
44. Mitchell, L. A.; Gao, J.; Wal, R. V.; Gigliotti, A.; Burchiel, S. W.; McDonald, J. D. Pulmonary and Systemic Immune Response to Inhaled Multiwalled Carbon Nanotubes. *Toxicol. Sci.* **2007**, *100*, 203–214.
45. Porter, D. W.; Hubbs, A. F.; Chen, B. T.; McKinney, W.; Mercer, R. R.; Wolfarth, M. G.; Battelli, L.; Wu, N.; Sriram, K.; Leonard, S.; et al. Acute Pulmonary Dose-Responses to Inhaled Multi-Walled Carbon Nanotubes. *Nanotoxicology* **2013**, *7*, 1179–1194.
46. Ma-Hock, L.; Strauss, V.; Treumann, S.; Kuttler, K.; Wohlleben, W.; Hofmann, T.; Groters, S.; Wiench, K.; van Ravenzwaay, B.; Landsiedel, R. Comparative Inhalation Toxicity of Multi-Wall Carbon Nanotubes, Graphene, Graphite Nanoplatelets and Low Surface Carbon Black. *Part. Fibre. Toxicol.* **2013**, *10*, 23.
47. Schinwald, A.; Murphy, F. A.; Jones, A.; MacNee, W.; Donaldson, K. Graphene-Based Nanoplatelets: A New Risk to the Respiratory System as a Consequence of Their Unusual Aerodynamic Properties. *ACS Nano* **2012**, *6*, 736–746.